Scanning Microscopy

Volume 10 | Number 3 Article 1

7-26-1996

Monte Carlo Simulation of Secondary Electron Emission From Thin Film/Substrate Targets

K. Murata
Osaka Prefecture University, murata@pe.osakafu-u.ac.jp

M. Yasuda
Osaka Prefecture University

H. Kawata
Osaka Prefecture University

Scanning Microscopy, Vol. 10, No. 3, 1996 (Pages 613-624) 0891-7035/96$5.00+.25
Scanning Microscopy International, Chicago (AMF O'Hare), IL 60666 USA

MONTE CARLO SIMULATION OF SECONDARY ELECTRON EMISSION FROM THIN FILM/SUBSTRATE TARGETS

K. Murata*, M. Yasuda and H. Kawata

Department of Physics and Electronics,
Osaka Prefecture University, Sakai, Osaka, Japan

(Received for publication March 5, 1996 and in revised form July 26, 1996)

Abstract

We have developed a Monte Carlo simulation model of secondary electron emission from thin film/substrate samples, taking into consideration their exact boundary condition. First, the validity of the model is checked in comparison with the experimental data reported such as the secondary electron emission and backscattering yields from thick Al, thick Au targets and Al thin films on a Au substrate, the energy distribution of secondary electrons, and the contribution of backscattering to the secondary electron emission yield. The agreement is relatively good. Next, we have applied the model to the secondary electron emission from Au films on an Al substrate. It has been found from the calculated results of the spatial distribution of secondary electrons that the Au film coating increases the background intensity and deteriorates resolution in the secondary electron image formation.

Key Words: Monte Carlo simulation, secondary electron emission, thin films on substrates, the spatial distribution of secondary electrons, backscattering contribution to the secondary electron yield.

*Address for correspondence:
Kenji Murata
Department of Physics and Electronics,
College of Engineering,
Osaka Prefecture University,
1-1 Gakuencho,
Sakai, Osaka 593, Japan
Telephone number: (81) 722-52-1161 ext. 2286
FAX number: (81) 722-59-3340
E-mail: murata@pe.osakafu-u.ac.jp

Introduction

Theoretical studies on secondary electron (SE) emission have been done by many authors. Among those studies, Monte Carlo simulation is very useful for studying the SE image formation in the scanning electron microscope because effects of electron diffusion are significant in complicated sample structures. Various Monte Carlo models have been proposed by many researchers. These models are classified typically into two types. One is based on the phenomenological treatment which assumes that the number of SEs generated is proportional to the energy deposited in a surface layer and that their escape probability is determined by the exponential decay, including the averaged inelastic mean free path of the electrons (Shimizu and Murata, 1971; Murata, 1973; Joy, 1984). The other is based on the cascade model, which tracks each electron generated by electron-electron collisions (Ganachaud and Cailler, 1973, 1979; Koshikawa and Shimizu, 1974; Kotera *et al.*, 1990a,b; Ding and Shimizu, 1996). The latter model is more realistic than the former. With the cascade model, some authors studied the SE image formation for various types of samples such as bulk samples, samples with a sharp edge, and step shape samples, etc. Koshikawa *et al.* (1974) investigated the energy distribution of SEs emitted from Be films of various thicknesses on Cu substrates with the cascade model. They assumed that the ratio of the excitation probability in Be and Cu is proportional to that of the SE yields for both the materials, and the inelastic mean free paths and the surface barriers are the same for both Be and Cu. However, more exact studies have not been done yet for samples with the thin film/substrate configuration with this model. The model is useful for a study of the SE image formation of thin film coated samples to prevent the charge-up effect. Also, it is useful for a study of the detectability of monolayers deposited on a substrate (for example, Ichinokawa *et al.*, 1981; Harland *et al.*, 1987).

In the present paper, we develop a Monte Carlo model of SE emission from thin film/substrate targets, taking account of the exact boundary condition and

applying it to the SE emission from Al film coated Au and Au film coated Al samples. The model is basically the same as those published by Koshikawa and Shimizu (1974) and Kotera *et al.* (1990a).

Monte Carlo Simulation Model

Modeling for elastic scattering and energy losses of the primary electron

A regular Monte Carlo simulation model is used for electron behavior of primary electrons in solid targets. A brief explanation is the following. An incident electron goes straight into a solid target. After passing a free path Δs, the electron suffers an elastic scattering event and then is deflected through an angle which is determined by the differential elastic cross section $d\sigma/d\Omega$. The free path is calculated by using a uniform random number R as follows:

$$\Delta s = -\Lambda \cdot \ln(R), \tag{1}$$

where Λ is the mean free path for elastic scattering. The value of Λ is given by

$$\Lambda^{-1} = \sigma^{tot} = \{\rho N_A / A\} \cdot \sigma, \tag{2}$$

where σ^{tot}: the total cross section for elastic scattering, A: atomic weight, ρ: the density, N_A: Avogadro's number and σ: the elastic scattering cross section per atom. The Mott cross sections are used for elastic scattering, which are given in a table as a function of energy (see Kotera *et al.*, 1981a,b).

An energy lost during traveling the free path is calculated by the following modified form of the Bethe law, which is proposed by Joy and Luo (1989):

$$\{-dE/ds\} = \{2\pi e^4 \rho N_A / AE\} \cdot Z\{\ln[1 + (1.166E/J)]\}, \tag{3}$$

where E: the primary electron energy, e: electron charge, Z: the atomic number and J: the mean ionization potential. The primary electrons are tracked until their energy slows down to 100 eV. The numbers of simulated trajectories are typically 5000 ~ 10000.

Modeling for true secondary electron emission

A cascade model of SE emission is similar to that proposed by Kotera *et al.* (1990a). But we introduced the average energy, ϵ, required to produce one SE. Namely, the energy loss is calculated in a step of the primary electron, divided by the value of ϵ and then the number of SEs generated is obtained. The value of ϵ is determined so that the calculated maximum SE yield matches to the experimental one. The position of generated SEs is assumed to be uniformly distributed along the electron path, and an emission angle is also uniform.

An energy, E_s, of the generated SEs is determined by the following Streitwolf formula (1959), which gives the energy excitation function for metal electrons bombarded by a primary electron beam.

$$S(E_s) = \{e^4 k_F^3\} / \{3\pi E_p (E_s - E_F)^2\}, \tag{4}$$

where e: electron charge, k_F: the Fermi wave vector, E_p: the primary electron energy, E_F: the Fermi energy. The function $S(E_s)$ can be used as the probability function to determine an energy, E_s, of generated SEs. Limiting the SE energy between E_c and $E_{spb} = E_F + \phi$, the energy of the SEs is obtained by using a uniform random number R.

$$E_s = \{RE_F - BE_{spb}\} / \{R - B\}, \tag{5}$$

where $B = (E_c - E_F)/(E_c - E_{spb})$ and ϕ: the work function. We assumed E_c = 100 eV. Thus, the electrons with energies less than 100 eV are handled by the cascade model.

The generated electron of energy E_s interacts with a conduction electron and scatters down in energy from E_s to E', resulting in production of a SE with the energy of E". For calculations of this energy separation, Koshikawa and Shimizu (1974) made use of the Wolff theory, which assumes spherically symmetric scattering in the center-of-mass system, taking into consideration the Pauli exclusion principle. According to their modeling, the energies E' and E" of scattered electrons and the scattering angle θ are given by:

$$E' = E_s R^{1/2} = E_s \cos^2\theta$$

$$E'' = E_s \sin^2\theta, \tag{6}$$

where E_s is the secondary electron energy before collisions and R is a uniform random number.

The inelastic mean free path of the secondary electrons is calculated by using the following empirical formula derived by Seah and Dench (1979):

$$\lambda = 538a(E_s - E_F)^{-2} + 0.41a^{3/2}(E_s - E_F)^{1/2}, \tag{7}$$

where a is the monolayer thickness in nm, given by

$$a^3 = \{A/\rho n N_A\} \cdot 10^{24}, \tag{8}$$

where A: the atomic weight, n: the number of atoms in the molecule, N_A: Avogadro's number and ρ: the density in $kg \cdot m^{-3}$. This equation is also used in a hybrid

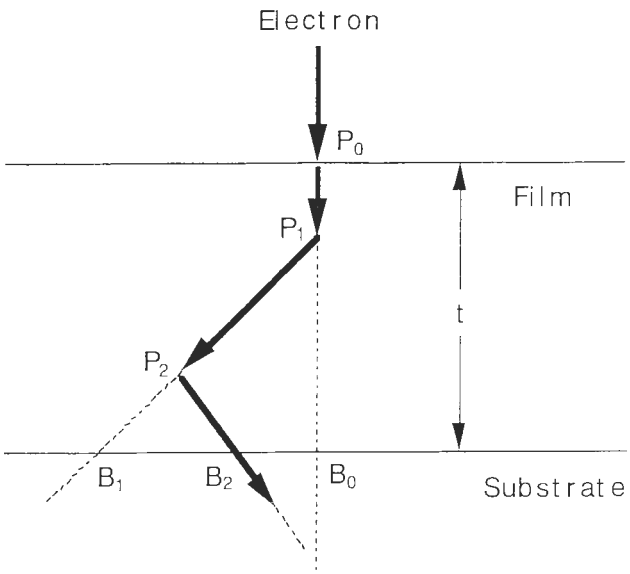

Figure 1. A schematic diagram showing the treatment of electron scattering at the film/substrate boundary.

model of the exponential decay law and cascade process (Luo and Joy, 1990).

Secondary electrons with energies between 0 and 50 eV are assumed to be the true secondary electrons. Thus, electrons with energies above 50 eV reflected from the sample surface are the backscattered electrons.

Note that the above model does not include the individual scattering processes of plasmons and inner shell excitations, and the angular distribution of SEs due to elastic scattering with nuclei.

These definitions yield the following relation:

$$\delta_{tot} = \delta_{true} + \eta, \qquad (9)$$

where δ_{tot}: the total SE emission yield, δ_{true}: the true SE emission yield and η: the backscattering coefficient.

The work functions and the Fermi energies used here are 4.25 eV and 11.80 eV for Al and 4.25 eV and 5.51 eV for Au, respectively, which are the same values as those by Kotera *et al.* (1990a).

Modeling for film/substrate targets

Since the mean free paths are usually different between a film and a substrate, a special consideration has to be taken for the scattering process. The exact treatment for such boundary has been already published before (Hawryluk *et al.*, 1982; Horiguchi *et al.*, 1981; Murata *et al.*, 1987). As shown in Figure 1, when the free path of the primary electron, which is generated in accordance with eq. (1), exceeds the boundary, a new free path has to be determined at the boundary B_n (n = 0, 1, 2,...) according to the following equation by using the same random number generated initially.

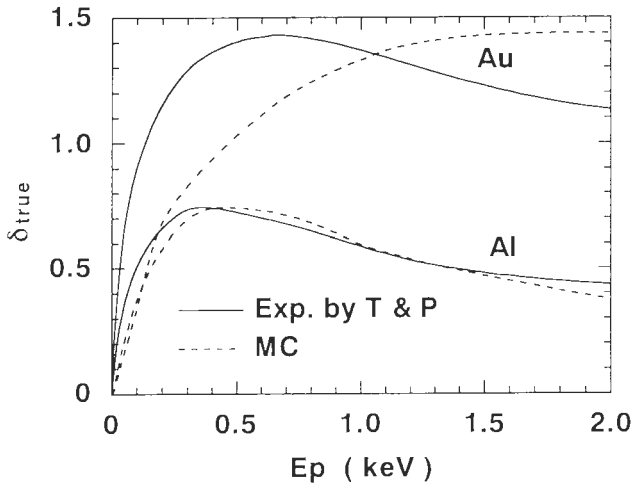

Figure 2. Comparisons of the true SE yield between Monte Carlo simulation and experiment by Thomas and Pattinson (1970) to find an energy ϵ required to generate one SE. The value of ϵ is found so that the peak value matches with the experimental one.

$$\Delta s = -\lambda_s\{(\lambda_f^{-1} - \lambda_s^{-1})\{l) + \ln(R)\} \qquad (10)$$

where λ_f and λ_s are the mean free paths in the film and in the substrate, respectively, l is a distance from the starting point of the step to the boundary and R is a uniform random number. This process is repeated whenever an electron crosses the boundary between the film and the substrate. When the electron goes from the substrate to the film, λ_f and λ_s have to be replaced with each other. The same treatment is done also for SEs.

Another thing to be considered when the electron crosses the boundary where there is a potential difference between both regions is the reflection or the refraction of the electrons. When the primary electron is incident on the target at an incident angle of α, the electron is refracted and goes toward the direction of an angle of γ, given by the following equation:

$$\{\sin\alpha / \sin\gamma\} = \{(E + E_{spb})/E\}^{1/2}, \qquad (11)$$

where E is a primary electron energy in vacuum.

But this effect at the boundary is neglected for the primary electron. Both the reflection and refraction effects are taken into account for SEs in a similar way to eq. (11). When crossing the boundary, an electron energy increases or decreases by the difference of the Fermi energies, since they coincide at the contact of the film and the substrate metals.

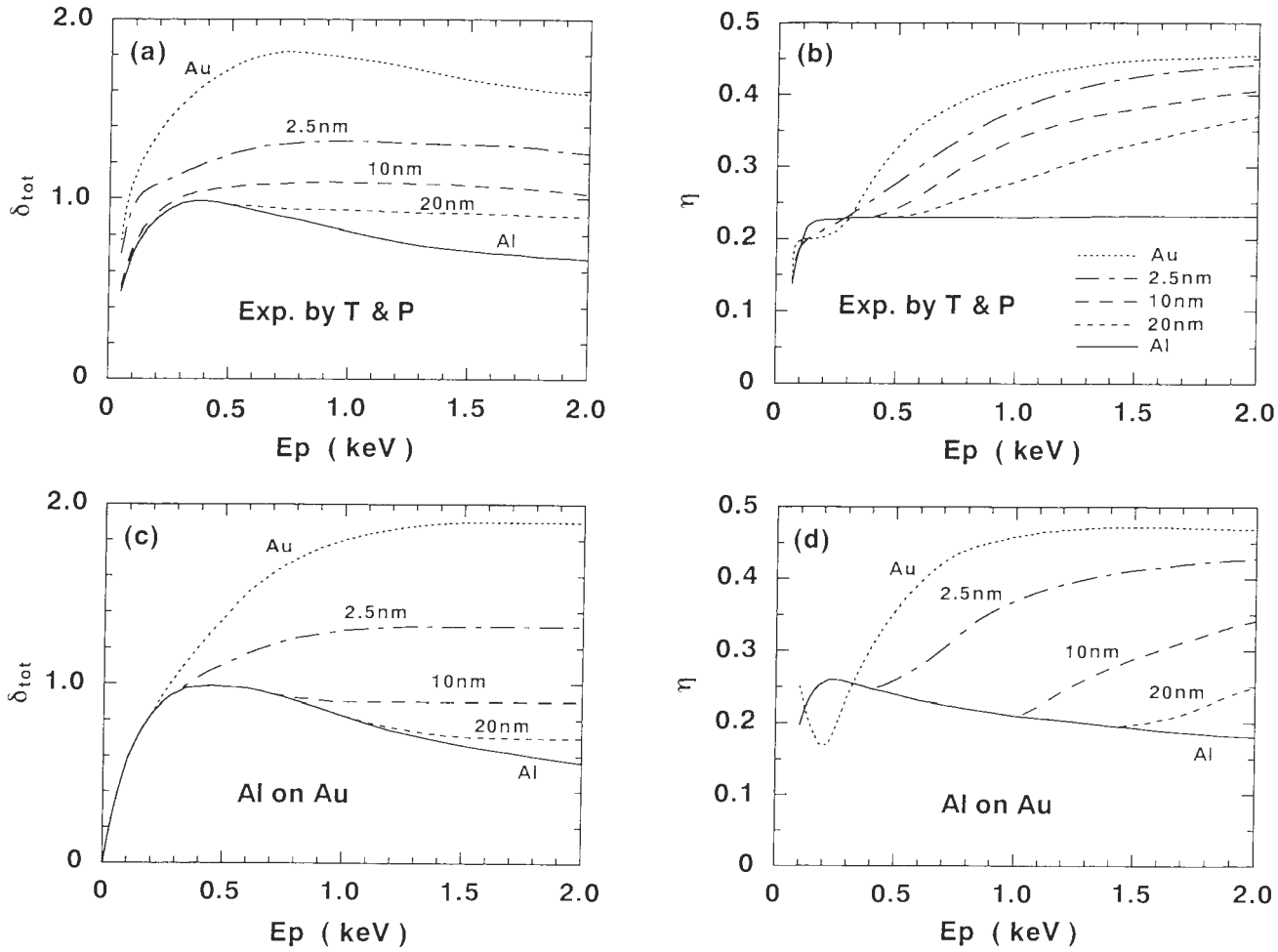

Figure 3. The primary electron energy dependences of the total SE yield and the backscattering yield for bulk Al and Au targets and thin Al films deposited on Au substrates. (**a**) and (**b**): experiment by Thomas and Pattinson (1970); (**c**) and (**d**): Monte Carlo results.

Results and Discussions

Secondary electron emission and backscattering from thin metallic films on substrates

Figure 2 shows the variations of δ_{true} with the primary electron energy, in comparison between calculation and experiment of Thomas and Pattinson (1970) for bulk Al and Au targets. The values of ϵ are 10 and 17.3 eV, which are obtained by matching the maximum values of the experimental true SE yields of 0.74 and 1.43 for Al and Au, respectively. As seen from the figure, reasonable agreement is obtained for Al, but not for Au. With the present model, it is possible to introduce new parameters in both the equations of the inelastic mean free path and the energy loss so as to match the calculated values to the experimental ones. Namely, either a decrease of the value of the inelastic mean free path or an increase of the energy loss makes the peak of the δ_{true} curve shift to a lower primary energy. But we have not done this because these physical quantities are still uncertain at the present. The problem is left unsolved. We should note that these quantities are very important and further studies are necessary.

In Figures 3a, 3b, 3c and 3d, the calculated values of δ_{tot} and η are shown as a function of the primary electron energy for bulk Al, bulk Au and Al thin films on Au substrates, compared with the experimental data of Thomas and Pattinson (1970). Three typical thicknesses are selected from the experimental data. Again, we can see another discrepancy between theory and experiment. Namely, both calculated curves for δ_{tot} and η for Al thin film coated samples deviate from those for the bulk Al sample at larger energies than the experimental ones. This means that the effect of the Au substrate comes out at larger energies, and that the theoretical electron penetration depth is underestimated or the

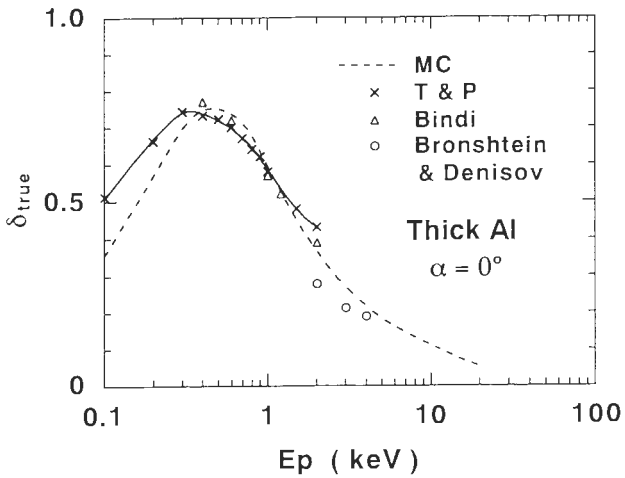

Figure 4. The primary electron energy dependence of the true SE yield for a bulk Al target. Monte Carlo results are compared with various experimental data.

---

energy loss is overestimated assuming that the experimental data are accurate. The Bethe electron range calculated by the energy loss law of Joy and Luo (1989) is larger by two or three times than that estimated experimentally by Thomas and Pattinson (1970) in the energy range of interest. This will be also an interesting subject in the future.

The calculated primary electron energy dependence of the true SE yield is shown for an Al bulk target in Figure 4, in comparison with the experimental data published (see Schou, 1988). The experimental result of Bindi (see Bindi *et al.*, 1987) agrees well with our result. The experimental results of Bronshtein and Denisov (1967) are not so far away from our Monte Carlo results. But the other experimental results by Kanter (1961), Shimizu (1974) and Reimer and Drescher (1977) give about two to three times larger values above the primary electron energy of 1 keV, although these data are not shown here.

Energy distribution of secondary electrons

In Figures 5a and 5b, the calculated energy distributions of SEs for Al and Au are shown at an energy of 1 keV, comparing with the experimental ones of Bindi *et al.* (1979), Roptin (1975) and Pillon (1974). A reasonable agreement is obtained for Au. But for Al, the full width of the half maximum (FWHM) of the distribution is smaller than those of both experiments. The main factors to determine the distribution are the source function of eq. (4) and the inelastic mean free path of eq. (7). The energy dependence of these factors is important. Kotera *et al.* (1990a) used the following empirical equation for Al, which is introduced for Cu by Koshikawa and Shimizu (1974):

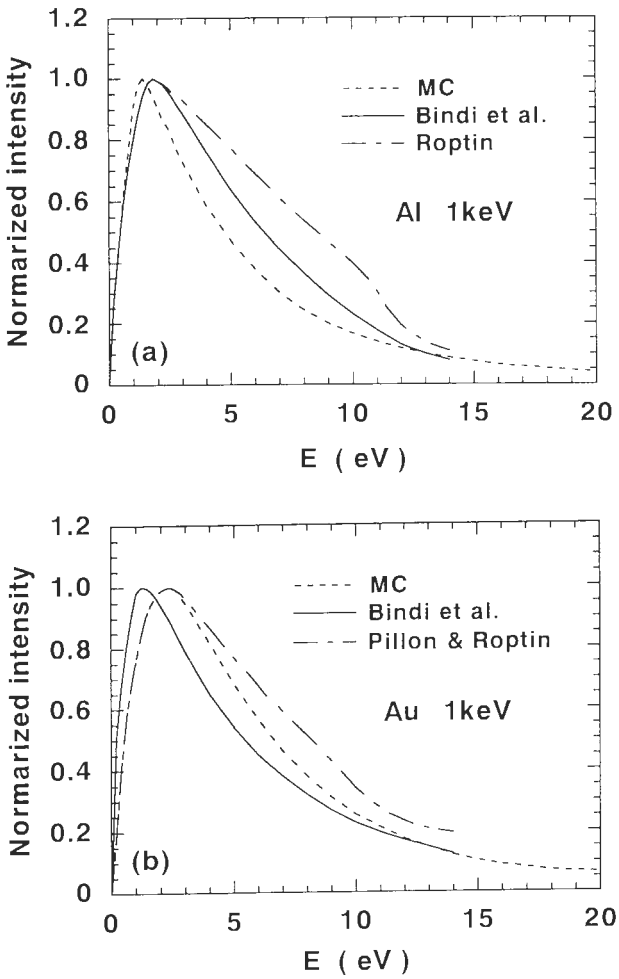

Figure 5. The energy distribution of SEs for bulk (**a**) aluminum and (**b**) gold targets at 1 keV. The Monte Carlo results are compared with the experimental data of Bindi *et al.* (1979), Roptin (1975) and Pillon (1974).

$$\lambda = 10^{(-2.6\ln(E) + 3.3)} \text{ nm, for } E \leq 25 \text{ eV}$$

and

$$\lambda = 0.5 \text{ nm, for } E > 25 \text{ eV}. \qquad (12)$$

The energy dependence of this mean free path is weaker for Al than that by Seah and Dench (1979) used in our model. Thus, with this formula, we can obtain a larger value of FWHM than ours. But we have not done this either.

Note that for more accurate studies of the energy distribution especially the plasmon excitation process has to be included (Rosler and Brauer, 1981).

Contribution of backscattering to the secondary electron yield

The primary electrons go straight forward into a sample while backscattered electrons are emitted in a diffused manner near the sample surface with smaller

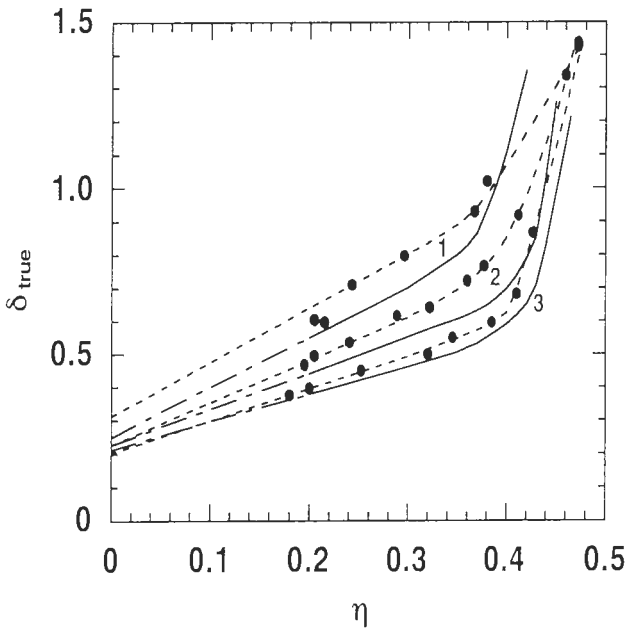

Figure 6. The δ_{true} versus η curve to find the SE production efficiency of one backscattered electron. Solid lines: experimental curve by Thomas and Pattinson (1970), and dashed lines: Monte Carlo results. 1: 1.0 keV, 2: 1.5 keV and 3: 2.0 keV.

---

energies than the primary electrons. Thus, the latter electrons are more efficient to produce secondaries than the former. The effect is formulated by the following equation:

$$\delta_{true} = \delta_p(1 + \beta\eta), \qquad (13)$$

where δ_p is the SE yield produced by the primary electron and β is the factor which represents the efficiency per one backscattered electron. Thomas and Pattinson (1970) derived the value of β from their experimental data of the SE yield from the Al thin films on the Au substrate as mentioned before. Namely, the β value is deduced from the slope of the δ_{true} versus η curve for various film thicknesses. In Figure 6, the curve plot is reproduced from their figure for energies of 1, 1.5 and 2 keV. Also, our calculated results are compared with experimental results. The curves rise up sharply near the η value of 0.35 because the substrate effect appears significantly. Below this value of η, the curve is almost linear and follows the eq. (13). The β values obtained with Monte Carlo calculations are 5.3, 5.1 and 4.8, and the experimental values are 6.3, 4.8 and 3.8 at energies of 1, 1.5 and 2 keV, respectively. These β values are similar to other reported experimental data (Bindi *et al.*, 1980, 1987). In spite of the discrepancies between theory and experiment mentioned before, relatively good agreement is obtained.

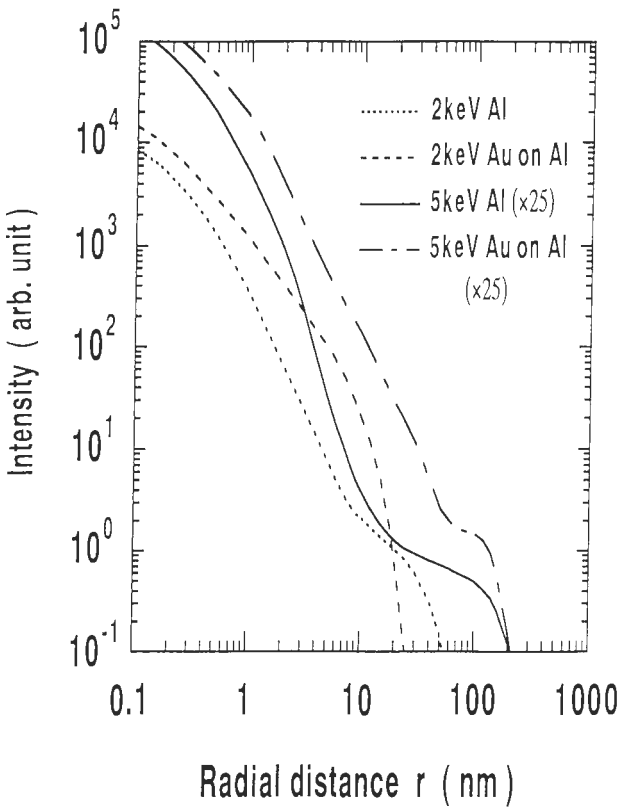

Figure 7. The calculated radial distributions of emitted SEs at 2 and 5 keV for bulk Al targets and Au films (10 nm) on Al substrates. The intensity for 5 keV is multiplied by 25 times.

Spatial distribution of true secondary electrons

When an insulator sample, such as a biological sample, is observed, metallic thin films are coated to prevent the charge-up. In such cases, the films are heavy element materials and the sample is usually light element materials. The above simulation can be applied to this case by replacing aluminum and gold materials. In this and following sections, we will study both the image resolution and the contrast of scanning electron microscopy for metallic thin films coated samples.

Figure 7 shows the calculated results of the spatial distribution of SEs at 2 and 5 keV for bulk Al targets and 10 nm Au films coated on Al substrates in a log-log plot. A zero-cross sectional beam is incident at a normal angle. For 5 keV, the intensity is multiplied by 25.

As seen in the figure, for the bulk samples, the distributions consist of two parts, that is, the distribution (called the peak distribution) where the contribution of the forward scattered electrons is dominant and the distribution produced by backscattered electrons which are diffused to large radial distances. The peak distribution near the incident point is included within a radius of

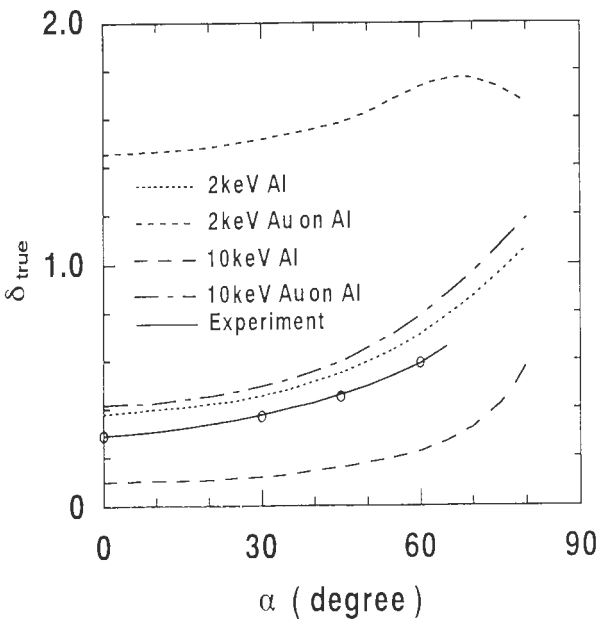

Figure 8. The Monte Carlo results of the beam incidence angle dependence of the true SE yield at 2 and 10 keV for bulk Al targets and Au films (10 nm) on Al substrates. The experimental results are after Bronshtein and Denisov (1967).

---

about 10 nm at both energies. The percentage of the intensities included within this area is 64% and 62% at energies of 2 and 5 keV, respectively. Since low energy SEs have the inelastic mean free path of several nanometers, the electrons produced by the forward scattered primary electrons may contribute to the distribution in this region. Especially within a radius of 1 nm, the distributions are close to the exponential decay. As a matter of fact, the distribution consists of a superposition of the contributions of the forward and the backward scattered primary electrons within these regions. The contribution of the total background intensity outside a radius of 10 nm is about 40%, due to large emission areas, although the intensity is very low.

The discrimination between the two parts mentioned above is not clear for the Au film coated sample at 2 keV. This is probably because the forward and the backward scattered electrons cannot be discriminated due to a large extent of electron diffusion. The peak distribution is broader and higher than that for the bulk sample.

At 5 keV, the peak distribution for the Au film coated sample extends to larger radial distances than that for the Al bulk sample. This is probably caused by both an increase in singly and plurally backscattered electrons from the Au thin film and a higher capability of the Au film for SE emission. About 82 percent of the total emission yield are included within a radius of 60 nm, where the transition occurs from the peak distribution to the background distribution.

If we plot the curves in a normal scale, we can see a sharp peak with the FWHM of about 0.2 nm around the incident point. This FWHM is much smaller than the value of 3 nm predicted by Joy (1984) for Al at 20 keV. His model is different from ours, but the fast secondary electron production may have to be taken into consideration especially at high energies as done by him. In any case, the radial distances where the intensity decreases down to one tenth of the peak intensity are within about one nanometer. If we assume that these radii give the resolution of the SE image, the remaining intensity outside this region will be the background. The percentages of the intensities included within a radius of 1 nm are 35% and 37% for the bulk samples, and 22% and 24% for the Au film coated samples at 2 and 5 keV, respectively. The corresponding values are 38% and 30% at 10 keV. These fractions do not change so much with the primary electron energy. It is naturally understood that the fraction is determined mainly by the backscattering yield, although the emission areas change largely. These values increase slightly with an increasing primary electron energy. The main reason for this is in that the backscattering yields decrease with an increasing energy and the backscattering contribution decreases. The yields, for example, for the bulk Al target, are 0.183, 0.170 and 0.156 at 2, 5 and 10 keV, respectively. It seems that the film coating decreases the percentage of the signal, which is effective to the SE image formation in high resolution observations.

Incidence angle dependence of the true secondary electron emission yield

The contrast of the SE image is basically determined by the incidence angle dependence of the true SE emission yield, although the contrast formation is not simple, as discussed by Pawley (1992). It will be an interesting subject to see the dependence for metallic film coated samples at low and high primary electron energies. Figure 8 shows the incidence angle dependence of the yield δ_{true} for Al bulk and 10 nm Au film coated samples at 2 and 10 keV. Figure 8 also shows the experimental result of Bronshtein and Denisov (1967) for an Al bulk target at 2 keV. Although the calculated yield gives a little higher values, the variation is similar to the experimental one. The variation for the Al bulk target at 10 keV is close to the inverse of $\cos\alpha$. The dependence is very weak for the Au film on the Al substrate at 2 keV, although this is not a practical case of SE observations. The reason of this weak dependence is that the effect of shallow incidence does not appear strongly due to a large extent of electron diffusion near the sample surface. On the other hand, the dependence for the same

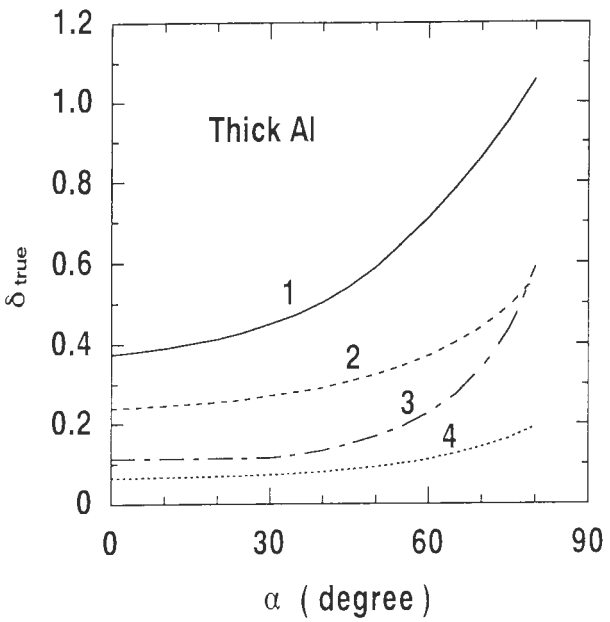

Figure 9. The incidence angle dependence of the true SE yields from the whole target area (curves 1 and 3) and the area within a radius of 10 nm (curves 2 and 4). Curves 1 and 2: 2 keV. Curves 3 and 4: 10 keV. The target is the bulk Al.

---

sample at 10 keV is similar to that for the Al bulk sample at 2 keV.

In observations of microstructures, a large portion of the contribution of backscattered electrons to the SE yield is the background in the image signal. Thus, the SE emission near the incident point of the primary electrons is important in the contrast generation of the image. To see the effect, the incidence angle dependence of the SE yield is calculated in the localized area within a radius of 10 nm. It is desired to integrate the intensities of the peak distribution of SEs which determine the contrast. But at oblique incidences, the distribution is not symmetrical about the beam incident point and it is tedious to find the distribution. Therefore, we selected tentatively the radius of 10 nm within which sufficient intensities are included even at oblique incidence. The results are shown in Figure 9 at 2 and 10 keV for the Al bulk sample, in comparison with the result from the whole area. The result for the Au film on the Al substrate at 10 keV is similar to that for the Al bulk sample at 2 keV, although it is not shown here.

We can see two things in Figure 9: (1) The decrease in the sample tilt angle contrast, especially at large angles. This means that the backscattered electrons contribute greatly to the tilt angle contrast produced by the SEs emitted from the whole area. The decrease is much larger at 10 keV than at 2 keV. But there is no large differences between the variations of the resulting curves 2 and 4. (2) The percentage of the background intensity due to backscattering to the total SE emission yield. The background intensities increase from 35% at normal incidence to 47% at 80 degrees and from 42% at normal incidence to 67% at 80 degrees at 2 and 10 keV, respectively. The background intensity is more significant at large incidence angles and high electron energies because more primary electrons go out at far distances from the incident point.

In the previous section, we have shown the spatial distribution for normal incidence. Here, let us show how the distribution changes with an incidence angle of the primary electron. In Figures 10a, 10b, 10c and 10d, the calculated lateral distributions of emitted SEs near the incident point are shown for bulk Al targets and 10 nm Au films on Al substrates at 2 keV and 10 keV. The results are shown for three typical incidence angles of 0, 30 and 60 degrees. The beam is in the x-z plane. The intensities are integrated over the direction of the y-axis. The calculated intensities are obtained in a subdivision of $x = 0.2$ nm, but the results are plotted as smooth curves. Although the intensities are shown in arbitrary units, they are compared with each other. For the bulk samples, the values of the FWHM of the distributions are 0.7, 1.0 and 3.1 nm at 2 keV, 0.6, 0.9 and 1.7 nm at 10 keV for the incidence angles of 0, 30 and 60 degrees, respectively. The corresponding values for the Au film coated samples are 0.9, 1.7 and 3.5 nm at 2 keV, and 0.7, 1.4 and 4.5 nm at 10 keV, respectively.

It is natural in any cases that the peak intensity decreases and the distribution becomes broader with an increasing angle.

For the bulk, the distribution at 2 keV is broader than that at 10 keV, particularly at larger incidence angles, because the diffusion of electrons with lower energies starts at shallower depths.

At 10 keV, the distribution for the Au film on the Al substrate is much broader than that for the bulk Al target at oblique incidences. The FWHMs do not differ so much from each other at normal incidence. The reason why the difference does not appear between them is the following. The peak distribution is formed mainly by the SEs produced by primary electrons right after incidence at high energies. Thus, for the Au film coated sample, the SEs produced within the 10 nm film are dominant. On the other hand, the inelastic mean free paths expressed by eq. (7) do not differ so much between Al and Au for SEs emitted with the same energies, although their energies inside the targets are different due to the difference of the surface potentials or the Fermi energies in the present case. It is because the inelastic mean free paths are given for energies above the Fermi energy.

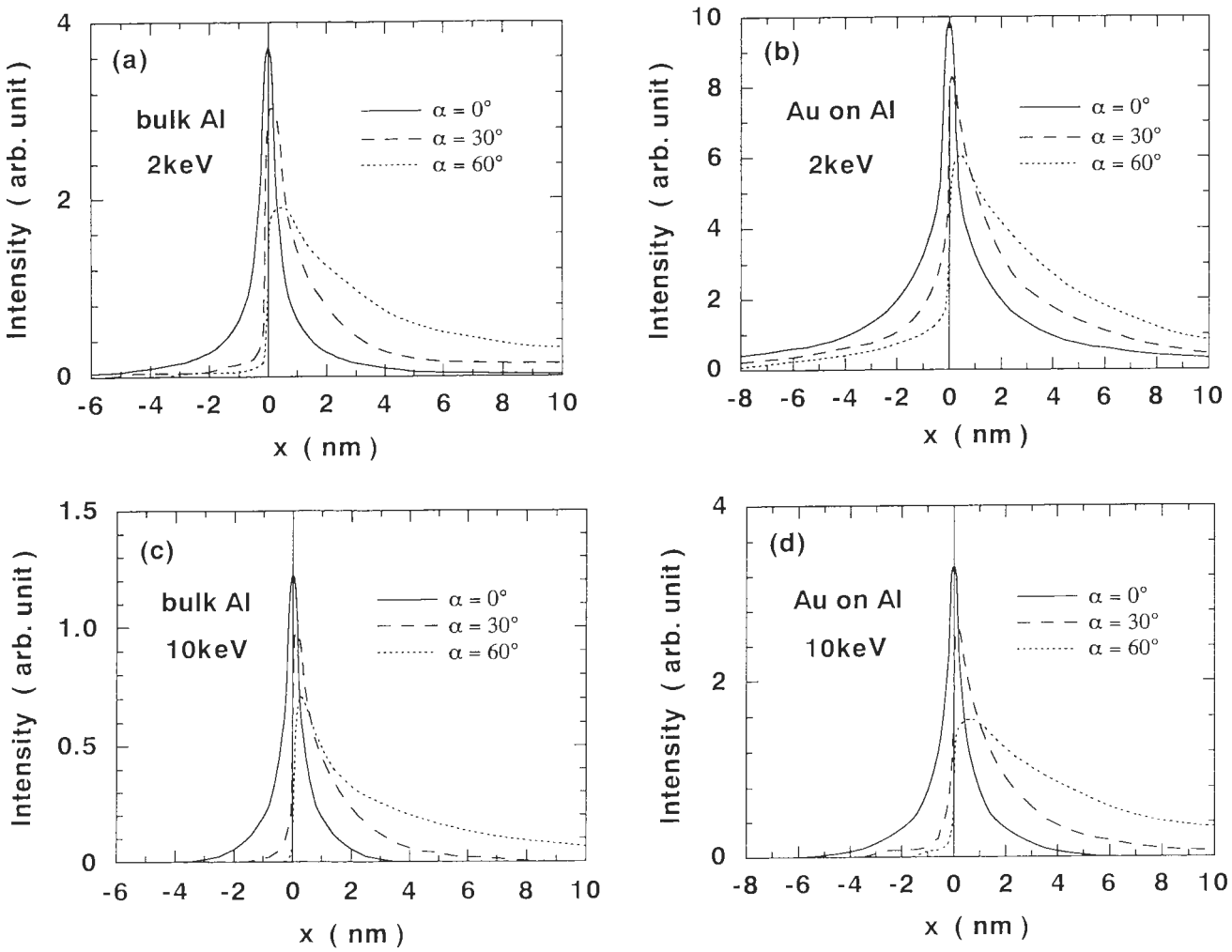

Figure 10. Calculated lateral distributions of SEs. (**a**) 2 keV, bulk Al; (**b**) 2 keV, Au film (10 nm) on Al; (**c**) 10 keV, bulk Al; and (**d**) 10 keV, Au film (10 nm) on Al.

Conclusions

A Monte Carlo model developed for SE emission from thin film/substrate targets has been checked in comparison with the published experimental data such as the primary electron energy dependence of the SE yield, the energy distribution of SEs. Although generally good agreement is obtained, some discrepancies are found in the results of the SE and the backscattering yields from Al thin films on Au substrates as a function of the primary electron energy. This suggests that we need further investigations on the energy loss law and the inelastic mean free path. Nevertheless, the above calculations give useful knowledge that the coating film to prevent the charge-up effect increases the SE emission yield in the background and deteriorates the image resolution.

References

Bindi R, Lanteri H, Rostaing P (1979) Distributions énergétiques expérimentales des électrons secondaires émis par des cibles évaporées d'aluminium, de cuivre, d'or et d'argent (Experimental energy distribution of secondary electrons emitted by evaporated targets of aluminum, copper, gold and silver). J. Electron. Spect. Rel. Phen. **17**, 249-258.

Bindi R, Lanteri H, Rostaing P, Keller P (1980) Theoretical efficiency of backscattered electrons in secondary electron emission from aluminium. J. Phys. D: Appl. Phys. **13**, 2351-2361.

Bindi R, Lanteri H, Rostaing P (1987) Secondary electron emission induced by electron bombardment of poly-crystalline metallic targets. Scanning Microsc. **1**,

1475-1490.

Bronshtein IM, Denisov SS (1967) Secondary electron emission of aluminum and nickel for obliquely incident primary electrons. Sov. Phys.: Solid St. **9**, 731-732.

Ding ZJ, Shimizu R (1996) A Monte-Carlo modeling of electron interaction with solids including cascade secondary electron production. Scanning **18**, 92-113.

Ganachaud JP, Cailler M (1973) Traitement Unifie de L'Emission Electronique Secondaire du Cuivre par Une Methode de Monte Carlo (Unified treatment of secondary electron emission from copper by a Monte Carlo method). J. de Physique **34**, 91-98.

Ganachaud JP, Cailler M (1979) A Monte-Carlo calculation of the secondary electron emission of normal metals. Surf. Sci. **83**, 498-530.

Harland CJ, Jones GW, Doust T, Venables JA (1987) Scanning electron microscopic observations of monolayer deposits using biassed secondary electron and specimen current imaging. Scanning Microsc. Suppl. **1**, 109-114.

Hawryluk RJ, Hawryluk AM, Smith HI (1982) Addendum: New model of electron free path in multiple layers for Monte Carlo simulation. J. Appl. Phys. **53**, 5985.

Horiguchi SM, Suzuki M, Kobayashi T, Yoshino H, Sakakibara Y (1981) New method of electron free path in multiple layers for Monte Carlo simulation. Appl. Phys. Lett. **39**, 512-514.

Ichinokawa T, Ishikawa Y, Agawa N, Onoguchi A (1981) Analytical scanning electron microscopy in UHV for solid surface. Scanning Electron Microsc. **1981**; I, 271-283.

Joy DC (1984) Beam interactions, contrast and resolution in the SEM. J. Microsc. **136**, Pt 2, 241-258.

Joy DC, Luo Suichu (1989) An empirical stopping power expression for low energy electrons. Scanning **11**, 176-180.

Kanter H (1961) Contribution of backscattered electrons to secondary electron formation. Phys. Rev. **121**, 681-684.

Koshikawa T, Shimizu R (1974) A Monte Carlo calculation of low-energy secondary electron emission from metals. J. Phys. D: Appl. Phys. **7**, 1303-1315.

Koshikawa T, Goto K, Shimizu R, Ishikawa K (1974) Secondary electron energy spectra from a Be layer evaporated on Cu. J. Phys. D: Appl. Phys. **7**, L174-L177.

Kotera M, Murata K, Nagami K (1981a) Monte Carlo simulation of 1-10 keV electron scattering in a gold target. J. Appl. Phys. **52**, 997-1003.

Kotera M, Murata K, Nagami K (1981b) Monte Carlo simulation of 1-10 keV electron scattering in an aluminum target. J. Appl. Phys. **52**, 7403-7408.

Kotera M, Kishida T, Suga H (1990a) Monte Carlo simulation of secondary electrons in solids and its application for scanning electron microscopy. Scanning Microsc. Suppl. **4**, 111-126.

Kotera M, Ijichi R, Fujiwara T, Suga H, Wittry DB (1990b) A Simulation of Electron Scattering in Metals. Jpn. J. Appl. Phys. **29**, 2277-2282.

Luo S, Joy DC (1990) Monte Carlo calculations of secondary electron emission. Scanning Microsc. Suppl. **4**, 127-146.

Murata K (1973) Monte Carlo calculations on electron scattering and secondary electron production in the SEM. Scanning Electron Microsc. **1973**; II, 267-276.

Murata K, Kawata H, Nagami K, Hirai Y, Mano Y (1987) Studies of energy dissipation in resist films by a Monte Carlo simulation based on the Mott cross section. J. Vac. Sci. Technol. **B5**, 124-128.

Pawley JB (1992) LVSEM for high-resolution topographic and density contrast imaging. In: Advances in Electronics and Electron Physics. Hawkes P (ed.). Academic Press, San Diego, CA. pp. 203-273.

Pillon J (1974) Etude critique d'un spectroscope Auger pour l'émission électronique secondaire - Résultats obtenus sur un cristal de Cu (111) (Critical studies of an Auger spectrometer - Results obtained from a Cu (111) crystal). Thèse de Docteur-Ingénieur (Doctoral thesis), Université de Nantes, France.

Reimer L, Drescher H (1977) Secondary electron emission of 10-100 keV electrons from transparent films of Al and Au. J. Phys. D: Appl. Phys. **10**, 805-815.

Roptin D (1975) Etude expérimentale de l'émission électronique secondaire de l'Aluminium et de l'Argent (Experimental study of secondary electron emission from aluminum and silver). Thèse de Docteur-Ingénieur (Doctoral thesis), Université de Nantes, France.

Rosler M, Brauer W (1981) Theory of secondary electron emission II. Application to Aluminum. phys. stat. sol. (b) **104**, 575-587.

Schou J (1988) Secondary electron emission from solids by electron and proton bombardment. Scanning Microsc. **2**, 607-632.

Seah MP, Dench WA (1979) Quantitative electron spectroscopy of surfaces: A standard data base for electron inelastic mean free paths in solids. Surf. Interf. Analy. **1**, 2-11.

Shimizu R (1974) Secondary electron yield with primary electron beam of kilo-electron-volts. J. Appl. Phys. **45**, 2107-2111.

Shimizu R, Murata K (1971) Monte Carlo calculations of the electron-sample interactions in the scanning electron microscope. J. Appl. Phys. **42**, 387-394.

Streitwolf HW (1959) Zur Theorie der Sekundarelektronen Emission von Metallen: Der Anregungsprozess (The theory of secondary electron emission

from metals: The excitation process). Ann. Phys. (Leipz.) **3**, 183-196.

Thomas S, Pattinson EB (1970) Range of electrons and contribution of back-scattered electrons in secondary production in aluminium. J. Phys. D: Appl. Phys. **3**, 349-357.

Discussion with Reviewers

J.R. Lowney: The theory of secondary generation is very complicated because of the attempt to include quantum-mechanical effects for low-energy electrons in a theory that is primarily based on high energy formalism. Please discuss the accuracy of secondary-electron modeling in light of this fact.

D.C. Joy: Your model for secondary generation predicts a full width at half maximum of 0.2 nm. Since Monte Carlo models assume that the material in which they are applied is a continuum ("jellium") could you comment on whether or not predictions made about effects at atomic levels (i.e., 0.2 nm) are likely to be valid?

Authors: Since a regular Monte Carlo method pursues the electron trajectories as a particle, the results obtained here are surely classical ones. Assuming an energy of 15 eV for SEs inside a metal, the de Broglie wavelength of those electrons will be about 0.3 nm. This exceeds the distance at atomic levels as you anticipated. Therefore, the present results give only a rough idea how broad SEs are emitted spatially. Any quantum mechanical consideration must be taken into account in the future.

D. Hasselkamp: Is there a measurable influence of the metal film on the overall energy distribution of emitted electrons in your model?

Authors: Yes. As an example, the energy distributions of SEs from Al films on Au substrates are shown in Figure 11 for various thicknesses at a primary electron energy of 2 keV. As you can see, the FWHMs of the distributions get smaller with an increasing thickness, reach the minimum at around 4 to 6 nm and increase toward that of the bulk Al target. This result is similar to that obtained by Koshikawa *et al.* (1974) for Be films on Cu substrates. The reason for this behavior, as already explained by Koshikawa *et al.* (1974), is in the fact that SEs emitted from deeper depths have lower energies on average, and more SEs are emitted from the substrates.

J. Schou: As far as I read the paper, the elastic scattering is included for the primary electron, but not for the secondary electrons. What is the influence of elastic scattering processes on the secondary electrons within the model? How does it modify the yield of the true electrons?

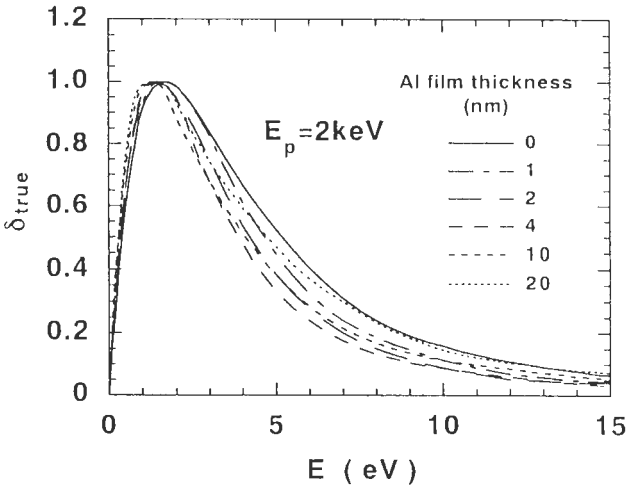

Figure 11. The variation of the energy distribution of SEs with thickness of Al films on Au substrates.

Authors: A similar question is already answered in "Discussion with Reviewers" in the paper by Kotera *et al.* (1990a), responding to D.C. Joy. Since the angular distribution of SEs shows the cosine curve, it is said that the random scattering process dominates for the SEs in a sample. This means that the direction of motion of the SEs is lost. Therefore, it is speculated that the inclusion of an anisotropic angular distribution due to elastic scattering does not affect their behavior significantly. However, we do not know actually how the elastic scattering process of slow SEs influences the SE emission. The SE yield is calculated by adjusting the value of ϵ. If such an effect exists, the inclusion of elastic scattering may change the value of ϵ. Wolff (1954) also neglected this effect in his theoretical work, but pointed out that a strong crystal field has to be investigated further.

D.C. Joy: You note that "the Bethe range calculated from the energy loss law of Joy and Luo is larger by two to three times than that estimated experimentally by Thomas and Pattinson." Recent experimental measurements of electron stopping power in the materials used in these calculations generally show agreement within $\pm$ 10% of the values predicted by the Joy and Luo equation. Can you comment on other possible reasons for the observed discrepancy?

Authors: Both experimental and theoretical errors may be considered. As seen in Figures 3b and 3d, the discrepancy is seen in the backscattering yield curves which are easier to observe than the SEs. Although thin film measurements seem to be most difficult, Thomas and Pattinson say the measurements are done with an accuracy of $\pm$ 10%. Their maximum range is about 85 nm while the Bethe range calculated from eq. (3) (Joy and

Luo, 1989) is about 40 nm for Al at 1 keV. It should be noted that various experimental data of the electron range tend to show the latter value at 1 keV (Kotera *et al.*, 1981b), as you commented.

Theoretically, we do not take account of the energy straggling due to the discrete energy loss process which makes the electron range longer. Further investigations are needed for this process. But, we do not think even the inclusion of this effect can account for such large differences.